Interaction Dynamics Between Ferroelectric and Antiferroelectric Domains in a PbZrO_{3}-Based Ceramic

Zhongming Fan, Fei Xue, Goknur Tutuncu, Long-Qing Chen, and Xiaoli Tan

Phys. Rev. Applied **11**, 064050 — Published 21 June 2019

DOI: 10.1103/PhysRevApplied.11.064050

Interaction dynamics between ferroelectric and antiferroelectric domains in a $PbZrO_3$-based ceramic

Zhongming Fan,[1] Fei Xue,[2] Goknur Tutuncu,[1] Long-Qing Chen,[2] and Xiaoli Tan[1*]

[1] *Department of Materials Science and Engineering, Iowa State University, Ames, IA 50011, USA*

[2] *Department of Materials Science and Engineering, Pennsylvania State University, University Park, PA 16802, USA*

Abstract

The antiferroelectric-ferroelectric phase transition in $PbZrO_3$-based oxides is of both fundamental and practical importance. In ceramics that such a transition readily occurs, the antiferroelectric and the ferroelectric phases often coexist in individual grains with a coherent interphase interface. In this work, the electric biasing *in situ* transmission electron microscopy technique is employed to directly observe a unique microstructural dynamic when ferroelectric and antiferroelectric domains are driven by a moderate electric field to interact. It is found that, under monotonic loading, the ferroelectric domain grows until it is blocked by the ferroelectric/antiferroelectric interface. At the same time, a kink is formed on the interface at the contact point. The interaction of the growing domain with the interface is interpreted in terms of depolarization field-assisted phase transition, which is supported by our phase-field simulation. Upon further bipolar cycling, the ferroelectric domain becomes less mobile and no longer reaches the ferroelectric/antiferroelectric interface, indicative of electric fatigue of the ferroelectric phase.

---

*Author to whom correspondence should be addressed. Electronic mail: xtan@iastate.edu

I. INTRODUCTION

The domain dynamics under applied electric field (E_{appl}) is crucial to understanding the macroscopic phenomena observed in ferroelectric (FE) or antiferroelectric (AFE) crystals. In FE materials, the polarization tends to align with the external E field, realized through the domain switching process [1,2]. In AFE compounds [3,4], on the other hand, AFE→FE phase transition receives much more attention as AFE domains are nonpolar and do not directly respond to applied fields [5]. Meanwhile, in some AFE materials with certain compositions, both AFE and FE phases can coexist, either in separate grains or in single grains [5,6]. As a result, the electric field induced AFE→FE phase transition occurs more readily, making these compositions suitable for devices such as electrocaloric coolers or electromechanical actuators [7,8]. However, the interaction between the FE and AFE domains under E_{appl}, even though unavoidable in these compositions during service, has rarely been discussed.

$PbZrO_3$-based compositions are the most studied AFE ceramics and their AFE/FE phase equilibrium can be effectively tuned via chemical modifications with Ti and Sn, along with minor amounts of La or Nb [9,10]. For instance, the solid solution $Pb_{0.99}Nb_{0.02}[(Zr_{0.57}Sn_{0.43})_{1-y}Ti_y]O_3$ (abbreviated as PNZST 43/100y/2) is in single FE phase at room temperature for $y \geq 0.09$, single AFE phase for $y < 0.05$, and mixed FE and AFE phases in between [10]. Generally speaking, the critical field for FE domain switching is lower than that for the AFE→FE transition in AFE ceramics (E_F). Therefore, there exists a window for E_{appl} that only switches the FE domains but does not trigger the phase transition in compositions of $0.05 < y < 0.09$ with mixed phases. It can be expected that the microstructural dynamics under such an intermediate E_{appl} will involve the interactions between FE and AFE domains. Apparently, such microstructural dynamics is distinct from either the pure FE domain switching process or the AFE→FE phase

transition. It is toward this unique physics problem we select PNZST 43/6/2 as a model system with AFE phase as the main phase and the FE phase as the minor phase. The electric biasing *in situ* transmission electron microscopy (TEM) is employed to directly reveal the dynamic interactions between FE and AFE domains.

II. EXPERIMENTAL PROCEDURE

The PNZST 43/6/2 ceramic was prepared using the solid state reaction method. Raw powders with purity better than 99.9% of PbO, Nb_2O_5, ZrO_2, SnO_2, and TiO_2 were batched according to the chemical formula with 5% excess PbO powder to compensate for the lead evaporation loss in the subsequent thermal process. The powders were calcined at 850 ^oC for 4 hours in a covered alumina crucible for two times to ensure the chemical homogeneity and the phase purity. Sintering was performed at 1300 ^oC for 3 hours with $PbZrO_3$ protective powder. After the pellet was ground and electroded, the electric field-induced strain (*S*-*E*) measurement was performed. The detailed setup was described elsewhere [11].

Bulk specimens with dimensions of 1.0×0.9×6.0 mm^3 were prepared for the *in situ* synchrotron X-ray diffraction study, which was conducted at the Advanced Photon Source, Argonne National Laboratory. The *in situ* TEM experiments were conducted on FEI Tecnai G2-F20 at room temperature. As-sintered pellets were mechanically ground and polished to 120 μm thickness. Disks of 3 mm in diameter were ultrasonically cut and the center portion was thinned to 10 μm by mechanical dimpling. The dimpled disks were annealed at 200 ^oC for 2 hours to minimize the residual stress before Ar-ion milling to perforation. During the *in situ* TEM fatigue test, bipolar electric fields in a triangular waveform with a frequency of 0.1 Hz were applied.

III. RESULTS

Figure 1(a) displays a grain with coexisting AFE and FE phases viewed along the $[001]_c$ zone-axis. The AFE/FE interface runs from lower left to upper right with both phases containing two domains. The FE phase, with an inclusion domain embedded in a large matrix domain, displays only fundamental spots in its selected electron diffraction pattern [12]. The AFE phase contains two domains with different contrasts and the selected electron diffraction pattern recorded from the domain wall region (white circle) shows two orthogonal sets of satellite spots, indicative of the orthogonal arrangement of incommensurate modulations in the two AFE domains [13]. This gain has an ideal morphology to study the interaction of a growing FE domain with an AFE domain. Since the rest part of this grain (grain size ~ 5 μm) is farther away from the interface, it is not imaged in this experiment.

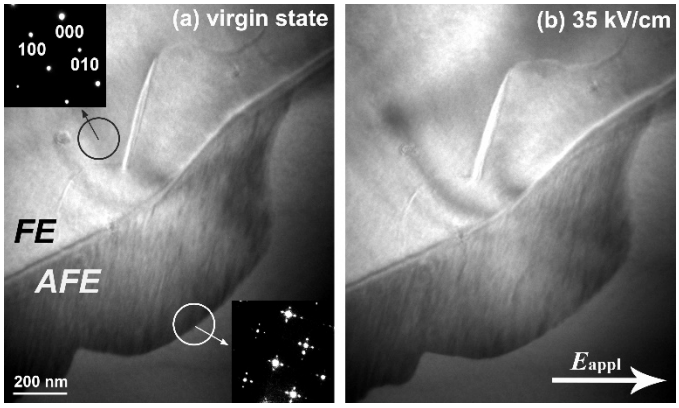

Fig. 1. The grain of interest, imaged along the $[001]_c$ zone axis, with coexisting AFE and FE phases in PNZST 43/6/2 at (a) virgin state, (b) 35 kV/cm. The insets in (a) show the electron diffraction patterns recorded from highlighted areas. The bright arrow in (b) indicates the direction of E_{appl}.

The evolution of this area under E_{appl} is subsequently monitored. The bright arrow in Fig. 1(b) marks the direction of the initial field loading. At 35 kV/cm, no apparent changes in microstructure are observed. Then, the polarity of E_{appl} is reversed [Fig. 2]. At the amplitude of

25 kV/cm, the embedded inclusion FE domain is observed to grow primarily lengthwise before it reaches the AFE/FE interface and is blocked [Fig. 2(b)]. As E_{appl} continues to increase, further growth of the FE domain proceeds with an apparent lateral widening. More importantly, the AFE/FE interface is poked towards the AFE side until a right angle is formed between the rotated AFE/FE interface and the long FE domain [Fig. 2(c)]. The dark triangles in Fig. 2 mark a point defect cluster, presumably immobile under the applied fields in this experiment. Using this feature as a reference point, the displacement of the AFE/FE interface can be more clearly appreciated. It should be noted that 35 kV/cm is chosen again to be the peak field for the purpose to reveal the asymmetric response of the microstructure under E_{appl} of the same amplitude but opposite polarities. Meanwhile, no noticeable changes have been detected in the AFE phase away from the interface, indicating that the AFE to FE phase transition only takes place at the preexisting AFE/FE interface. Once the E_{appl} is removed, the AFE/FE interface rotates back to its original position and the inclusion FE domain resumes its initial size as well [Fig. 2(d)]. This shows that the AFE↔FE phase transition and the FE domain switching in the minor FE phase are both reversible in PNZST 43/6/2.

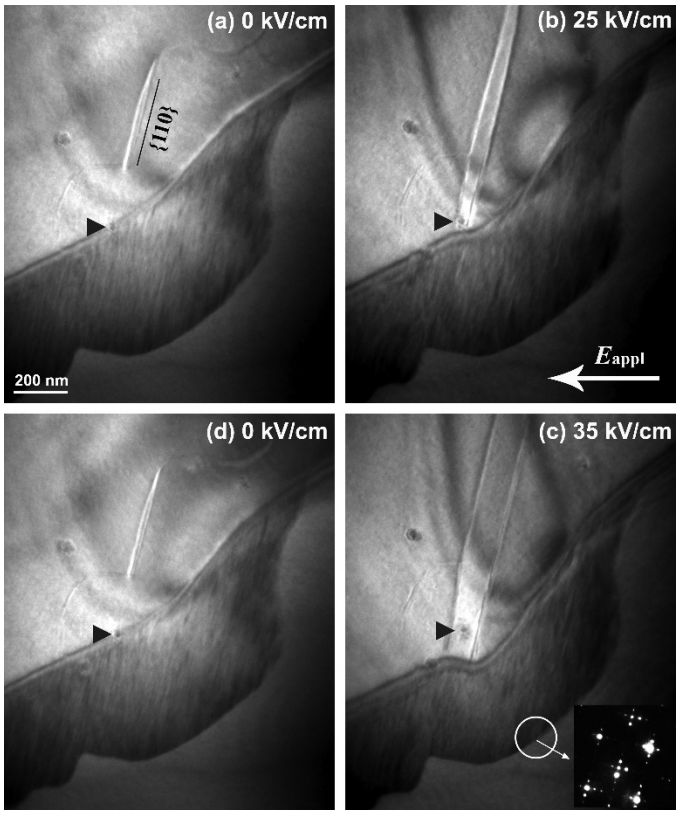

Fig. 2. The microstructural evolution during the monotonic electric field loading with the polarity opposite to Fig. 1. The micrographs are taken at (a) 0 kV/cm, (b) 25 kV/cm, (c) 35 kV/cm, and (d) back to 0 kV/cm. The dark triangles mark a defect cluster which is used as a reference point to reveal the displacement of the AFE/FE interface. The edge-on wall of the inclusion FE domain is on the $\{110\}_c$ plane.

Then the responses of the FE and AFE domains to bipolar cyclic fields of ±35 kV/cm are focused (Fig. 3). After 100 cycles, it is found that the AFE/FE interface slightly shifts upward [Fig. 3(a)]. When a DC field of 35 kV/cm (same polarity with Fig. 2) is applied [Fig. 3(b)], the inclusion FE domain grows lengthwise, but is apparently shorter and thinner than that under the first field application [Fig. 2(c)]. The AFE/FE interface retrieves to its original position while being slightly poked. After 1000 cycles, the AFE/FE interface seems to continue shift upward [Fig. 3(c)]. At a DC field of 35 kV/cm, very minor growth of the inclusion FE domain takes

place and the AFE/FE interface again retrieves to its original position. Previously, some macroscopic investigations on the electric fatigue in AFE ceramics claimed that either AFE or FE phase can be stabilized during cycling [14-16]. Microscopically, this may be manifested in the shift of the AFE/FE interface towards either direction. However, the exact mechanism is still unclear at this moment, hence requires more detailed investigations.

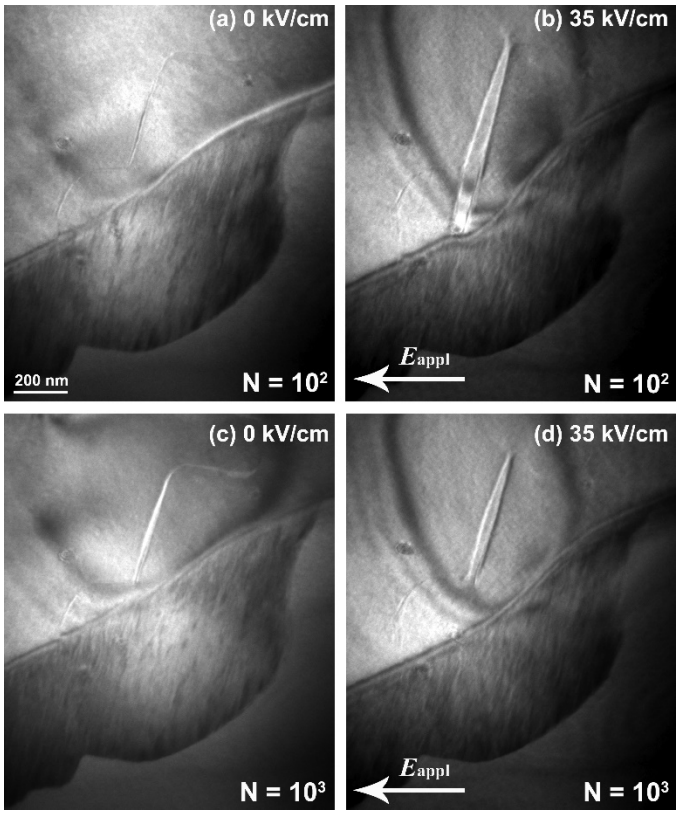

Fig. 3. Monitoring the fatigue degradation under bipolar applied fields of ±35 kV/cm after (a) and (b) 10^2 cycles, (c) and (d) 10^3 cycles. (a) and (c) show the domain morphology when the applied field is removed, while (b) and (d) are recorded under an applied field of 35 kV/cm.

IV. DISCUSSION

A. FE domain dynamics

The responses of the inclusion FE domain to the applied field could imply the polarization directions in the FE phase. It is well known that an E_{appl} is able to switch the polarization in FE domains via nucleation and growth of new domains [1,2], or via expansion of existing domains with favored polarization at the expense of those unfavored [17]. Assisted by this principle and the rhombohedral symmetry of the FE phase, the crystallographic information of the experimental results in Fig. 2 can be elaborated in Fig. 4. Considering that the polarizations are along $<111>_c$ directions in the rhombohedral phase, the most likely polarization directions for both matrix and inclusion domains are projected onto the $(001)_c$ observation plane, represented by the bright arrows in Fig. 4(a). Under the situation in Fig. 2, the lenticular inclusion FE domain serves as a seed with the favored polarization direction. As a consequence, the inclusion FE domain grows and expands at the expense of the matrix domain.

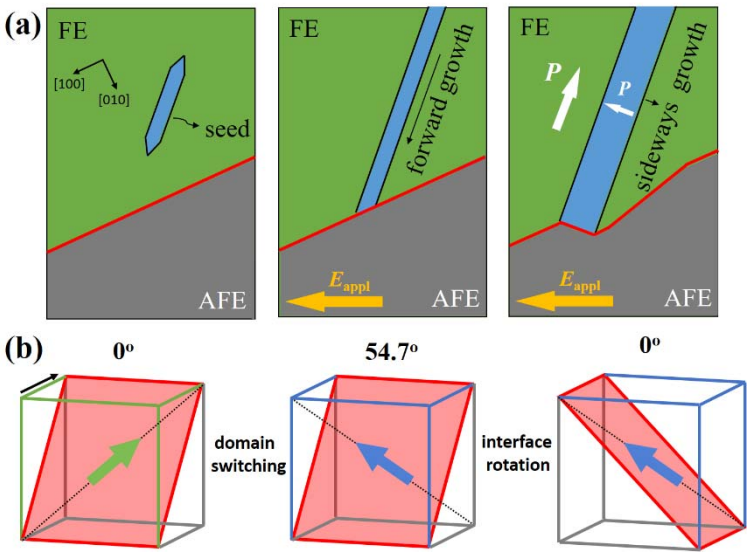

Fig. 4. (a) Schematic diagrams to illustrate the experimental observations in Fig. 2. (b) 3D illustration of the evolution of the angle between the FE polarization (green/blue arrows) and the AFE/FE interface (red plane) when the blue domain is in contact with, then has poked to rotate the AFE/FE interface. The small black arrow along the upper left edge of the cube denotes the viewing direction in TEM.

However, it should be noted that the walls between the matrix FE domain and the inclusion FE domain are not electrically neutral. The associated electrostatic energy not only makes the growth of the inclusion domain difficult, but also assists the recovery of the initial size upon removal of E_{appl}. This explains why the FE domain switching observed in Fig. 2 is slow and reversible. In addition, the fatigue degradation (Fig. 3) might also be ascribed to the charged FE domain walls. As with other normal FE ceramics, the mobility of a charged domain wall decays fast during cycling with bipolar electric fields [18,19]. Particularly in PNZST 43/6/2, the non-neutral FE domain walls may gradually trap charged point defects (most likely O vacancies) and the growth of FE domain becomes more difficult. After 1000 cycles, the accumulated point defects pin the domain walls and prevent the domain from growth (Fig. 3d).

Apparently, the growth of the inclusion FE domain is driven by E_{appl}, of which the amplitude, combining Fig. 1 and Fig. 2, is known nonetheless insufficient to trigger the AFE to FE phase transition. This is further evidenced by the strain vs. electric field hysteresis loop data measured on a bulk PNZST 43/6/2 specimen where E_F is determined to be roughly 40 kV/cm (Fig. 5). The *in situ* X-ray diffraction experiments on a bulk specimen also indicate that PNZST 43/6/2 under $E_{appl} < 40$ kV/cm is in AFE phase best fitted with the *Bmm2* space group of lattice parameters of $a = 5.8246$ Å, $b = 4.1000$ Å, $c = 5.8378$ Å (0 kV/cm), while in the induced FE phase under $E_{appl} >$ 40 kV/cm and is best fitted with the *R3c* space group of $a = 5.8282$ Å and $c = 14.2878$ Å (at ~56 kV/cm). From the *in situ* TEM results shown in Fig. 2, the majority of the AFE phase does not change under E_{appl}. The observation seems to suggest that the asymmetric responses under bipolar fields (Figs. 1 and 2) may not be resulted from the aged AFE phase [20]. Therefore, E_{appl} = 35 kV/cm indeed lies in the field window that only switches the FE domain but does not trigger a general AFE→FE transition. However, it should be pointed out that the AFE to FE

phase transition does take place locally, manifested as the displacement of the AFE/FE interface in Fig. 2(b) and (c). Such localized transition is attributed to the fact that the growing FE domain intersects with the interphase interface. This also explains why the AFE/FE interface cannot rotate anymore once the FE domain loses its mobility and does not reach the interface (Fig. 3).

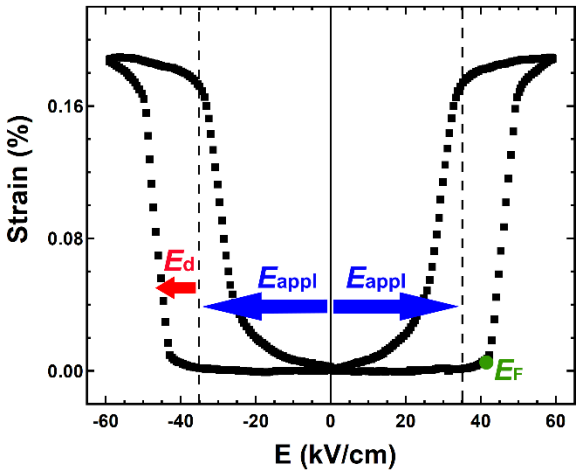

Fig. 5. The strain vs. electric field hysteresis loop measured on a bulk PNZST 43/6/2 ceramic.

B. E_d assisted AFE to FE phase transition

Depolarization field (E_d) exists near electrodes or FE domain walls if the polarization-induced bound charges are not fully compensated [21,22]. Presumably, the interface between the polar FE phase and the non-polar AFE phase should also be a location bearing E_d. It is known that an uncompensated E_d is likely to lead to morphology instability, e.g. the minimization of depolarization energy (U_d) accounts for the breakage of a single domain into multiple smaller domains, as U_d is quantitatively proportional to the domain width [23]. Given the fact that the original AFE/FE interface is stable, it must be close to a crystallographic plane with minimal E_d. According to this condition, the 3D configuration of the AFE/FE interface is schematically illustrated in Fig. 4(b), with the electron beam direction pointing from the front to the back. Originally, the AFE/FE interface lies on a $\{110\}_c$ plane (red). The polarization of the matrix FE

domain is along the <111>$_c$ direction (green arrow) in-plane with the interface. After the inclusion FE domain intersects with the interface, its polarization (blue arrow) forms a 54.7^o angle with the interface, accompanied with the emergence of an uncompensated E_d. In order to minimize the U_d, the AFE/FE interface has to rotate until it becomes in-plane with the switched polarization. A stable AFE/FE interface segment is hence established; before which the uncompensated E_d has assisted the AFE to FE phase transition at a local scale. In other words, the contact of the growing inclusion FE domain with the AFE/FE interfaces generates E_d; E_{appl} and E_d act in synergy (Fig. 5) and trigger the AFE to FE transition by displacing/rotating the AFE/FE interface [1,24]. Apparently, E_d itself is not sufficient to maintain the induced FE phase, so AFE phase is restored after E_{appl} is removed.

We also employ phase-field simulations to elucidate the origin of this local phase transition. To describe the AFE to FE phase transition, the model includes two sets of order parameters, polarization $P_i(i=x,y,z)$ and AFE orders $q_i(i=x,y,z)$. The AFE order parameter q_i is defined by the difference of two-sublattice polarizations, i.e., $\vec{q}=\frac{1}{2}(\overrightarrow{P_a}-\overrightarrow{P_b})$, where $\overrightarrow{P_a}$ and $\overrightarrow{P_b}$ are polarizations of two sublattices [25,26]. The total free energy is given by

$$\begin{aligned} F=\int_V [&\alpha_{ij}P_iP_j+\alpha_{ijkl}P_iP_jP_kP_l+\alpha_{ijklmn}P_iP_jP_kP_lP_mP_n \\ &+\beta_{ij}q_iq_j+\beta_{ijkl}q_iq_jq_kq_l+\beta_{ijklmn}q_iq_jq_kq_lq_mq_n+t_{ijkl}P_iP_jq_kq_l \\ &+\frac{1}{2}g_{ijkl}\frac{\partial P_i}{\partial x_j}\frac{\partial P_k}{\partial x_l}+\frac{1}{2}\kappa_{ijkl}\frac{\partial q_i}{\partial x_j}\frac{\partial q_k}{\partial x_l}-E_iP_i-\frac{1}{2}\varepsilon_0\kappa_bE_iE_i]dV \end{aligned} \quad (1)$$

where $\alpha_{ij},\alpha_{ijkl},\alpha_{ijklmn},\beta_{ij},\beta_{ijkl},\beta_{ijklmn}$, and t_{ijkl} are the coefficients for the Landau free energy function, g_{ijkl} and κ_{ijkl} are the coefficients for the gradient energy terms, x_i is the spatial coordinate, E_i is the electric field, ε_0 is the permittivity of free space, and κ_b is the background permittivity [27]. With coupling term coefficients t_{ijkl} sufficiently positive, P_i and q_i are

competitive with each other. Since there is no report for the Landau energy coefficients for PNZST, we use the Landau coefficients of the FE and AFE phases for the Sm-doped $BiFeO_3$ system [27]. Note that the Sm-doped $BiFeO_3$ system shows similar relative stabilities of FE and AFE phases as the PNZST system due to the similar change of the tolerance factor (The tolerance factor is given by $t = (R_A + R_O)/\sqrt{2}(R_B + R_O)$, where R_A, R_B, and R_O are the ionic radii of the A and B cations, and O anion, respectively) [27-29]. Therefore, we expect similar AFE to FE phase transition dynamics in the two systems. Also, the phase transition dynamics from phase-field simulations are insensitive to the specific values of Landau energy coefficients. In this study, we focus on the AFE to FE phase transitions, and the coefficients producing similar relative FE and AFE energies will give rise to similar domain structure evolutions in the simulations. This is also the case experimentally, i.e., two systems at the same position relative to the FE-AFE phase boundaries should show similar phase transition behaviors under external electric fields, which may be regarded as one type of universality. From the lattice parameter of the FE *R3c* phase, the shear strain component of the phase transformation strain in the pseudocubic coordinate system is smaller than 0.03%, and we expect that the elastic energy makes small contributions to the domain wall orientation. Thus the elastic energy term is neglected in Eq. (1), compared to a typical ferroelectric phase-field model [30]. It is assumed that the gradient energy coefficient tensor g_{ijkl} and κ_{ijkl} are isotropic. Therefore, the orientation of FE domain walls and FE/AFE interface is determined by the minimization of the electrostatic energy.

The phase-field equations for P_i and q_i are solved with periodic boundary conditions along three directions [31]. The system size is $256\Delta x \times 256\Delta x \times 256\Delta x$, and the grid spacing is $\Delta x = 1.0\, nm$. The initial condition is the coexistence of a FE domain and an AFE domain with a

charge-free interface, and a FE inclusion domain is artificially added within the FE domain, as shown in Fig. 6(a). To simulate the FE/AFE interface pinning effect, the AFE order parameter in the regions far away from the inclusion is fixed. Then we apply a constant electric field, which favors the FE inclusion domain over the FE matrix domain.

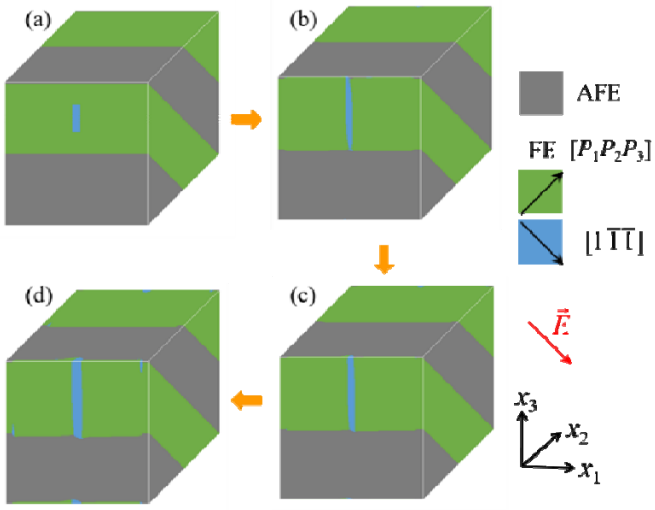

Fig. 6. Evolution of domain structures from a phase-field simulation. (a) Initial domain structure. An inclusion FE domain is added within the FE matrix domain. (b)-(d) Domain structures at 2,500, 4,500, and 8,000 simulation steps. A constant electric field is applied, with its direction labelled by the red arrow. The AFE phase and the two FE domains are labelled by different colors, and the polarization directions are labelled by the black arrows.

The temporal evolution of domain structures from a phase-field simulation is given in Fig. 6(b)-6(c). As shown in Fig. 6(b), the FE inclusion domain grows primarily lengthwise until it reaches the FE/AFE interface. Then the FE/AFE interface neighboring the inclusion domain is rotated by ~45°, as demonstrated in Fig. 6(c). In a phase-field model described by Eq. (1), the interface orientation is determined by the minimization of the electrostatic energy. The local distortion of the FE/AFE interface is, hence, driven by the electric field in the vicinity of the

intersecting point. Afterwards, the main growth mode of the FE inclusion domain is lateral widening as in Fig. 6(d). Therefore, even incapable of perfectly reproducing the observed morphology, the phase-field simulation has confirmed our hypothesis that the AFE to FE phase transition near the intersection of the grown FE domain and the AFE/FE interface is actually assisted by E_d.

V. CONCLUSIONS

In summary, a unique microstructural dynamic during the interaction between the FE and AFE domains in a $PbZrO_3$-based AFE ceramic under an intermediate E field is directly visualized with *in situ* TEM. It is found that, when the FE domain reaches the AFE/FE interface, the emerged depolarization field is able to assist triggering the AFE to FE phase transition at a local region by introducing distortions to the AFE/FE interface. In the initial electric cycle, both the FE domain growth and the phase transition are reversible and all the microstructure changes are recovered when the field is unloaded. However, the mobility of the FE domain is significantly suppressed after further bipolar cycling due to fatigue degradation. The results not only reveal a new scenario of electric field driven microstructural evolution, but also shed light on the complex nature of phase transitions in ferroic crystals.

ACKNOWLEDGEMENTS

The National Science Foundation (NSF), through Grant No. DMR-1700014, supported the experimental work. The phase field simulation work is supported by the U.S. Department of Energy, Office of Basic Energy Sciences, Division of Materials Sciences and Engineering under Award FG02-07ER46417 (FX and LQC), and by the National Science Foundation under DMREF Grant DMR-1629270 (FX).

[1] P. Gao, J. Briston, J.R. Jokisaari, C. T. Nelson, S. -H. Baek, Y. Wang, C.-B. Eom, L. -Q. Chen, and X. Pan, Atomic-scale mechanisms of ferroelectric domain-wall-mediated ferroelectric switching, Nat. Commun. **4**, 2791 (2013).

[2] C. T. Nelson, P. Gao, J. R. Jokisaari, C. Adamo, A. Melville, S. -H. Baek, C. M. Folkman, B. Winchester, Y. Gu, Y. Liu, K. Zhang, E. Wang, J. Li, L. -Q. Chen, C. -B. Eom, D. G. Schlom, and X. Pan, Domain dynamics during ferroelectric switching, Science **334**, 968 (2011).

[3] I. Zamaraite, R. Yevych, A. Dziaugys, A. Molnar, J. Banys, S. Svirskas, and Y. Vysochanskii, Double hysteresis loops in proper uniaxial ferroelectrics, Phys, Rev. Appl. **10**, 034017 (2018).

[4] G. A. Sewvandi, D. Hu, C. Chen, H. Ma, T. Kusunose, Y. Tanaka, S. Nakanishi, and Q. Feng, Antiferroelectric-to-ferroelectric switching in $CH_3NH_3PbI_3$ perovskite and its potential role in effective charge separation in perovskite solar cells, Phys. Rev. Appl. **6**, 024007 (2016).

[5] H. Guo and X. Tan. Direct observation of the recovery of an antiferroelectric phase during polarization reversal of an induced ferroelectric phase, Phys. Rev. B **91**, 144104 (2015).

[6] L. Gao, H. Guo, S. Zhang, and C. A. Randall, A perovskite lead-free antiferroelectric x$CaHfO_3$-(1-x) $NaNbO_3$ with induced double hysteresis loops at room temperature, J. Appl. Phys. **120**, 204102 (2016).

[7] N. Novak, F. Weyland, S. Patel, H. Guo, X. Tan, J. Rödel, and J. Koruza, Interplay of conventional with inverse electrocaloric response in (Pb,Nb)(Zr,Sn,Ti)O_3 antiferroelectric materials, Phys. Rev. B 97, 094113 (2018).

[8] Z. Dai, Z. Xu, and Xi Yao, Effect of dc bias on pressure-induced depolarization of Pb(Nb,Zr,Sn,Ti)O_3 ceramics, Appl. Phys. Lett. **92**, 072904 (2008).

[9] K. Markowski, S. E. Park, S. Yoshikawa, and L. E. Cross, Effect of compositional variations in the lead lanthanum zirconate stannate titanate system on electrical properties, J. Am. Ceram. Soc. **79**, 3297 (1996).

[10] H. He and X. Tan, Raman spectroscopy study of the phase transitions in $Pb_{0.99}Nb_{0.02}[(Zr_{0.57}Sn_{0.43})_{1-y}Ti_y]_{0.98}O_3$, J. Phys. Condens. Matter **19** 136003 (2007).

[11] X. Tan, J. Frederick, C. Ma, E. Aulbach, M. Marsilius, W. Hong, T. Granzow, W. Jo, and J. Rödel, Electric-field-induced antiferroelectric to ferroelectric phase transition in mechanically confined $Pb_{0.99}Nb_{0.02}[(Zr_{0.57}Sn_{0.43})_{0.94}Ti_{0.06}]_{0.98}O_3$, Phys. Rev. B **81**, 014103 (2010).

[12] D. Viehland, Transmission electron microscopy study of high-Zr-content lead zirconate Titanate, Phys. Rev. B **52**, 778 (1995).

[13] Z. Xu, X. Dai, and D. Viehland, Impurity-induced incommensuration in antiferroelectric La-modified lead zirconate titanate, Phys. Rev. B 51, 6261 (1995).

[14] X. Liu and X. Tan, Suppression of the antiferroelectric phase during polarization cycling of an induced ferroelectric phase, Appl. Phys. Lett. **107**, 072908 (2015).

[15] X. J. Lou and J. Wang, Unipolar and bipolar fatigue in antiferroelectric lead zirconate thin films and evidences for switching-induced charge injection inducing fatigue, Appl. Phys. Lett. **96**, 102906 (2010).

[16] L. Zhou, A. Zimmermann, Y. -P. Zeng, and F. Aldinger, Bipolar electric fatigue behavior as a function of field strength in antiferroelectric (Pb,Ba,La)(Zr,Sn,Ti)O_3 ceramics, J. Mater. Sci. **39**, 2675 (2004).

[17] Y. W. Li, F. and X. Li, The effect of domain patterns on 180^o domain switching in $BaTiO_3$ crystals during antiparallel electric field loading, Appl. Phys. Lett. **104**, 042908 (2014).

[18] Z. Fan, C. Zhou, X. Ren, and X. Tan, Domain disruption and defect accumulation during unipolar electric fatigue in a BZT-BCT ceramic, Appl. Phys. Lett. **111**, 252902 (2017).

[19] H. Guo, X. Liu, J. Rödel, and X. Tan, Nanofragmentation of ferroelectric domains during polarization fatigue, Adv. Funct. Mater. **25**, 270 (2015).

[20] Z. Fan and X. Tan, In-situ TEM study of the aging micromechanisms in a $BaTiO_3$-based lead-free piezoelectric ceramic, J. Eur. Ceram. Soc. **38**, 3472 (2018).

[21] L. C. Tănase, L. E. Abramiuc, D. G. Popescu, A. -M. Trandafir, N. G. Apostol, I. C. Bucur, L. Hrib, L. Pintilie, I. Pasuk, L. Trupină, and C. M. Teodorescu, Polarization orientation in lead zirconate titanate (001) thin films driven by the interface with the substrate, Phys. Rev. Appl. **10**, 034020 (2018).

[22] Y. -B. Ma, B. -X. Xu, K. Able, and A. Grünebohm, Tailoring the electrocaloric effect by internal bias fields and field protocols, Phys. Rev. Appl. **10**, 024048 (2018).

[23] W. Y. Shih, W. -H. Shih, and I. A. Aksay, Size dependence of the ferroelectric transition of small $BaTiO_3$ particles: effect of depolarization, Phys. Rev. B **50**, 15575 (1994).

[24] A. Roelofs, N. A. Pertsev, R. Waser, F. Schlaphof, L.M. Eng, C. Ganpule, V. Nagarajan, and R. Ramesh, Depolarization-field-mediated 180 switching in ferroelectric thin films with 90 domains, Appl. Phys. Lett. **80**, 1424 (2002).

[25] F. Xue, L. Liang, Y. Gu, I. Takeuchi, S.V. Kalinin, L. -Q. Chen, Composition- and pressure-induced ferroelectric to antiferroelectric phase transitions in Sm-doped $BiFeO_3$ system, Appl. Phys. Lett. **106**, 012903 (2015).

[26] A. K. Tagantsev, K. Vaideeswaran, S. B. Vakhrushev, A. V. Filimonov, R. G. Burkovsky, A. Shaganov, D. Andronikova, A. I. Rudskoy, A. Q. R. Baron, H. Uchiyama, D. Chernyshov, A. Bosak, Z. Ujma, K. Roleder, A. Majchrowski, J. -H. Ko, and N. Setter, The origin of antiferroelectricity in $PbZrO_3$, Nat. Commun. **4**, 2229 (2013).

[27] F. Xue, L. Li, J. Britson, Z. Hong, C. A. Heikes, C. Adamo, D. G. Schlom, X. Pan, and L. -Q. Chen, Switching the curl of polarization vectors by an irrotational electric field, Phys. Rev B **94**, 100103 (2016).

[28] S. Karimi, I. M. Reaney, Y. Han, J. Pokorny, and I. Sterianou, Crystal chemistry and domain structure of rare-earth doped $BiFeO_3$ ceramics, J, Mater. Sci **44**, 5102 (2009).

[29] B. Jaffe, W. R. J. Cook, and H. Jaffe, Piezoelectric Ceramics (Academic Press, London, 1971).

[30] F. Xue, L. Li, J. Briston, Z. Hong, C. A. Heikes, C. Adamo, D. G. Schlom, X. Pan, and L. -Q. Chen,

Switching the curl of polarization vectors by an irrotational electric field, Phys. Rev. B **94**, 100103 (2016).

[31] L.-Q. Chen and J. Shen, Applications of semi-implicit fourier-spectral method to phase field equations, Comput. Phys. Commun. **108**, 147 (1998).